Calibration of multisatellite observations for climatic studies: Microwave Sounding Unit (MSU)

Norman C. Grody
Center for Satellite Applications and Research, NOAA/NESDIS, Camp Springs, Maryland, USA

Konstantin Y. Vinnikov
Department of Meteorology, University of Maryland, College Park, Maryland, USA

Mitchell D. Goldberg, Jerry T. Sullivan, and J. Dan Tarpley
Center for Satellite Applications and Research, NOAA/NESDIS, Camp Springs, Maryland, USA

Received 1 June 2004; revised 9 September 2004; accepted 27 September 2004; published 21 December 2004.

[1] The Microwave Sounding Units (MSU) aboard the NOAA series of polar orbiting satellites has been used by three groups to monitor the very small trend in the global tropospheric temperature over the 25-year satellite record. To obtain a homogeneous data set, each group made different calibration corrections of the MSUs in the form of fixed biases, and in some cases temperature-dependent adjustments, to each of the nine satellite instruments using data during the overlap periods. Up until now, however, the adjustments are empirically based. To improve the accuracy as well as our understanding of the error sources, this paper develops an alternate, physical approach for intercalibrating the MSU instruments. The paper develops a calibration model for the MSU instrument that includes the errors in the cold space and warm target measurements, as well as the nonlinear factor. Corrections for these calibration errors are estimated using a least squares minimization where the predictors are the differences between all 12 overlapping satellite measurements at low and high latitudes. After applying the calibration corrections, the zonally averaged differences between satellite instruments are no larger than 0.03 K, independent of latitude. It is also found that the tropospheric temperature trend derived from MSU measurements is nearly the same as the surface trend. Furthermore, it now appears that much of the earlier inconsistency between the satellite and surface measurements arises from errors in the MSU calibration correction procedure, which can artificially suppress the temperature trend. *INDEX TERMS:* 3360 Meteorology and Atmospheric Dynamics: Remote sensing; 6969 Radio Science: Remote sensing; 1894 Hydrology: Instruments and techniques; *KEYWORDS:* microwave remote sensing, temperature climate monitoring, Microwave Sounding Unit

Citation: Grody, N. C., K. Y. Vinnikov, M. D. Goldberg, J. T. Sullivan, and J. D. Tarpley (2004), Calibration of multisatellite observations for climatic studies: Microwave Sounding Unit (MSU), *J. Geophys. Res.*, *109*, D24104, doi:10.1029/2004JD005079.

1. Introduction

[2] Meteorological satellite observations are now available for periods longer than 25 yr, which means that they can be used effectively in climate change research. However, none of the existing long-term multisatellite records are homogeneous enough to be used for climate trend analysis. This inhomogeneity often arises from instrument changes and malfunctions, changes in satellite orbits and their evolution, gaps in observation because of lost satellites, and inadvertently erased or inefficiently archived data. Furthermore, most satellite programs were primarily designed to monitor short term weather variations for weather prediction, not for climate monitoring. To make the satellite data homogeneous, the observations must be intercalibrated against each other so that there is one unified multisatellite observing system. Overlapping observations of different satellites can be used for such a posteriori intercalibration of multisatellite records. Understanding the physical and statistical properties of the observed signal as well as physical theory and construction of the instrument is necessary to solve the problem of data homogenization and will be addressed here. Of all the satellite instruments flown in space, microwave radiometers are being used more extensively than any other sensor to monitor the long-term changes in temperature. We therefore chose this class of instrument for our study.

[3] For more than 30 years, a variety of microwave radiometers have been launched aboard Earth orbiting satellites to detect the upwelling thermal radiation emanating from the Earth's atmosphere and its underlying surface.

0148-0227/04/2004JD005079$09.00

The instruments have been used for measuring a wide range of surface and atmospheric parameters [e.g., *Grody*, 1993]. Of particular interest to meteorologists and climatologists is the temperature information available from these very unique instruments. The uniqueness comes from the ability of microwave radiation to penetrate clouds and the fact that the radiation in the 50 to 70 GHz oxygen region of the electromagnetic spectrum is directly proportional to the atmospheric temperature profile. The nearly all weather capability of microwaves improves the accuracy and spatial coverage of the temperatures derived from satellite measurements, and in fact prompted the National Oceanic and Atmospheric Administration (NOAA) to develop the first operational series of microwave radiometers in the mid 1970's. The instrument was called the MSU or Microwave Sounding Unit and has four channels within the oxygen region to profile the atmospheric temperature from the surface to the lower stratosphere. Besides the physical attributes, which lead to the development of the MSU, of critical importance for climate applications is the long term stability and precise spectral resolution of microwave radiometers which has been accurately reproduced by each MSU flown in space.

[4] The first MSU was launched in 1978 on a National Aeronautic and Space Administration polar orbiting satellite called TIROS-N. This instrument was followed later by a sequence of eight other launches on the NOAA series of polar orbiting satellites, until 1998 when the MSUs were replaced by the Advanced Microwave Sounding Unit (AMSU), which has more channels for sounding the atmospheric temperature with greatly improved accuracy. While the AMSU has made significant impact in improving the accuracy of numerical weather prediction, the series of nine MSU instruments has provided climatologists with more than 25 years of continuous data for monitoring the tropospheric and stratospheric temperature trends. In this paper we concentrate on the intersatellite calibration of the MSU instruments to provide a homogeneous data set.

[5] The 25 years of MSU satellite data have been used by three different groups [*Christy et al.*, 2003; *Mears et al.*, 2003; *Vinnikov and Grody*, 2003] to estimate the long-term, global atmospheric temperature trends. To construct a homogeneous data set from the nine different satellites, the measurements from all MSUs must be adjusted for their different observation times and intercalibrated to account for instrumental differences using data obtained during their overlap periods. Calibration adjustments take the form of fixed biases [*Vinnikov and Grody*, 2003] and in some cases, include temperature-dependent adjustments [*Christy et al.*, 2000; *Schabel et al.*, 2003]. However, large differences in the satellite measurements and climate results were found depending on the adjustments and the analysis procedure used to intercalibrate the different MSU instruments. To improve the accuracy of the MSU measurements, an improved calibration adjustment procedure is developed that accounts for the major sources of calibration error. Interestingly, this investigation was motivated when it was initially observed that the bias between MSUs on different satellites varied slightly with latitude. This latitudinal bias is discussed in section 4 and is shown to be directly related to errors in the nonlinearity and calibration target errors of the different instruments.

[6] While much has been written about the use of MSU data, comparatively little attention has been devoted to its calibration and in particular the uncertainties and error sources of calibration. The need for precisely accurate calibration is most important when monitoring the very small climatic changes of the Earth's temperature. However, in order to properly intercalibrate the MSUs aboard the different satellites it is necessary to develop an accurate calibration model characterizing the instrument that includes error terms. This paper develops the model and applies it to obtain calibration adjustments for all of the MSU instruments. Calibration adjustments are made for errors in the cold-space and warm target measurements as well as the uncertainties in the nonlinearity parameter. Since the satellites carrying MSUs are launched at different local solar times, it is also necessary to correct the measurements for diurnal temperature variations. This diurnal correction is not only important when using the full time series to derive the climatic trend but also important when determining the calibration adjustments using overlapping satellite measurements. It is for this reason that the paper examines the effects of diurnal variation on the MSU measurements in addition to the effects of calibration error.

[7] The physical basis of the MSU observations, including the effects of surface temperature and emissivity variations on the measurements, is reviewed in section 2. A physical calibration model is developed in section 3 that contains the adjustments of the MSU measurements for errors in the cold space and warm target measurements as well as the uncertainty in the instruments nonlinearity. These calibration adjustments are shown to be retrievable using a least squares minimization where the predictors are the differences between overlapping satellite measurements at low and high latitudes. The procedure is used in section 4 to obtain the adjustments for every MSU instrument and the results are evaluated.

2. Radiometer Response

[8] Microwave radiometers such as the MSU measure the thermal radiation emanating from the Earth's atmosphere and its underlying surface. At frequencies less than 300 GHz, the Planck function is accurately given by the Rayleigh-Jeans approximation so that the radiation intensity measured by a microwave radiometer is linearly proportional to the temperature at which an equivalent blackbody emits [*Janssen*, 1993]. This temperature is referred to as a brightness temperature, T_b, and is given by the radiative transfer equation

$$T_b(\nu,\theta) = T_u + \tau_S[\varepsilon_S T_S + R_S T_d] \quad (1)$$

where T_u is the upwelling atmospheric radiation reaching the satellite, T_d is the downwelling atmospheric radiation reaching the Earth's surface, T_S is the surface temperature, τ_S is the atmospheric transmittance along the satellite-Earth viewing path, R_S is the reflectivity and ε_S is the surface emissivity. For most applications the reflectivity can be approximately related to the emissivity using the specular relationship, $R_S = 1 - \varepsilon_S$. Except for surface temperature, all of the parameters in (1) are a function of the channel frequency, ν, and local zenith angle viewed on the Earth's

Table 1. Transmittance Parameters, P_ν and η, for Each MSU Channel[a]

Channel	Center Frequency, GHz	IF Bandwidth, MHz	P_ν, mbar	η
1	50.30	110	1721.7	1.845
2	53.74	110	608.9	1.608
3	54.96	110	308.3	1.604
4	57.95	110	88.9	2.097

[a]Also listed are the central frequency and half bandwidth for each channel.

surface, θ. As explained below, T_u is the dominant term in (1) for the frequency of interest, while the attenuated surface emission $\tau_S \epsilon_S T_S$ and attenuated downwelling reflected radiation $\tau_S R_S T_d$ are of secondary importance.

[9] One of the most important parameters is the transmittance function, which is the percent of energy attenuated by the atmosphere as the radiation propagates from an arbitrary pressure level above the Earth's surface to the satellite altitude. For the MSU frequencies within the 50 to 70 GHz oxygen absorption band, the transmittance function can be approximated as [*Grody*, 1993]

$$\tau(p) = e^{-X^\eta}, \quad \text{where} \quad X = \frac{p}{P_\nu \sqrt{Cos\theta}} \tag{2}$$

where p is an arbitrary pressure and the parameters P_ν and η are obtained by fitting the transmittance which the exact absorption model [*Rosenkranz*, 1993]. For reference, Table 1 lists the MSU channels, center frequencies, bandwidths and the transmittance parameters derived for each channel. Equation (2) is accurate to within 1% of the exact model calculations and can provide useful physical insight. For example, the total atmospheric transmittance, τ_S, contained in (1) is obtained from (2) by setting the pressure equal to the surface pressure, P_S, so that $\tau_S = \tau(P_S)$. Therefore, at sea level pressure, the transmittances for channels 2, 3, and 4 at nadir viewing are only 0.104, 0.001, and 0.000, respectively, so that the upwelling radiation in (1) becomes the dominant term, which is given as

$$T_u = \int_{\tau_S}^{1} T(p) d\tau = \int_{-\infty}^{\ln P_S} T(p) W(p;\nu,\theta) d\ln p \tag{3a}$$

where

$$W(p;\nu,\theta) = -\frac{d\tau(p)}{d\ln p}. \tag{3b}$$

(For reference, $T_d = \int_{\tau_s}^{1} T(p)\ d\ \ln\ \hat{\tau}$ where $\hat{\tau} = \tau_s/\tau(p)$.) The brightness temperature is then approximated by an integral whose integrand can be expressed in terms of the atmospheric temperature profile $T(p)$, multiplied by a Gaussian-shaped weighting function W which is a unique function of pressure, p, for a given frequency and zenith angle. Using (2) and (3b), the weighting function is

$$W(p;\nu,\theta) = \eta X^\eta e^{-X^\eta} \tag{4}$$

which peaks at pressure $P_\nu \sqrt{Cos\theta}$. Figure 1 shows the exactly calculated weighting functions at the nadir and extreme viewing angle for all of the MSU channels. Since we are interested in measuring the tropospheric temperature only, channel 2 is used. However, the MSU uses a cross-scan antenna to view Earth at five zenith angles (10.7°, 21.6°, 32.6°, 44.1°, 56.6°) on both sides of the nadir viewing position for which $\theta = 0°$. To eliminate the need for any angular corrections of the weighting function only nadir viewing measurements are used. As shown in Figure 1, the nadir weighting function for channel 2 peaks near 600 mb and extends from the surface to the lower stratosphere. Approximately 10 percent of the radiation resides above 150 mb since $1 - \tau(p = 150) \approx 0.10$, while another 10 percent arises from surface contributions since $\tau_S = \tau(p = 1013) \approx 0.10$. Therefore, while (3a) accounts for most of the brightness temperature measurement, the remaining terms in (1), which contains surface parameters, contributes about 10 percent of the radiation for MSU channel 2 at nadir. These residual contributions

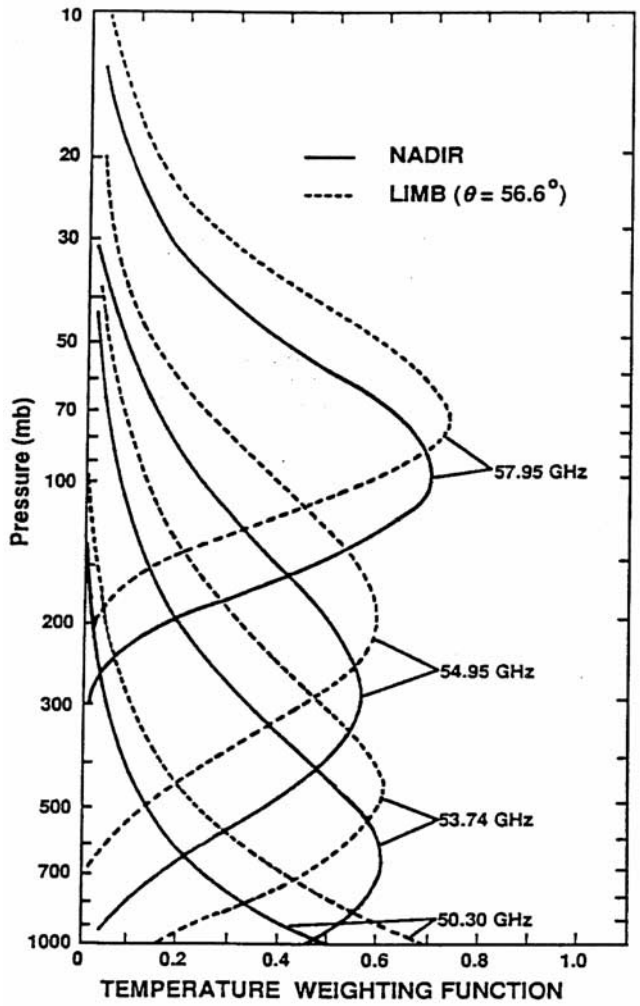

Figure 1. Weighting functions for the four MSU channel frequencies at the nadir and extreme limb position (θ is the local zenith angle). The center frequencies of 50.30, 53.74, 54.96, and 57.95 GHz are denoted as channels 1, 2, 3, and 4, respectively.

can present a number of problems when combining the different satellite observations. Foremost are the effects of diurnal temperature change and surface emissivity variations on the brightness temperature. As discussed in Appendix A, the emissivity effect can be significant over high elevation regions, but it is minimal and requires no adjustments for global climatic analysis. Of greater importance is the diurnal effect, which must be corrected for.

[10] Diurnal variations of brightness temperature arise mainly from changes in the surface temperature, ΔT_S. The diurnal variation in brightness temperature, ΔT_b, seen by the different MSU instruments is then approximately given by the term $\tau_S \varepsilon_S T_S$ in (1) so that

$$\Delta T_b = \tau_S \varepsilon_S \quad \Delta T_S. \tag{5}$$

For example, a 10 K diurnal variation in surface temperature can result in a 1 K difference in the MSU measurements on two satellite platforms that view the Earth at different local solar times. Equation (5) when combined with (2) also shows that decreased surface pressure due to increased land elevation increases the transmittance and consequently results in larger diurnal variations in brightness temperature. Incidentally, in contrast to the diurnal variations, which are mainly apparent near the surface, the longer term seasonal changes modify the temperature profile throughout much of the atmosphere. As such there is generally a strong correlation between seasonal variations, surface temperature and brightness temperature variations, i.e., $\Delta T_b \approx \Delta T_S$.

[11] Extensive analysis was performed by *Vinnikov and Grody* [2003] to examine the importance of diurnal corrections on the derived instrumental biases and climatic trend. To study this issue the 25 years of MSU measurements were represented by a Fourier series that contains the diurnal variations, seasonal variations and linear trend in addition to the instrumental biases, which were considered constant. Since the diurnal period is 24 hours, all odd diurnal harmonics can be eliminated by averaging the ascending and descending satellite measurements, which are 12 hours apart. This is important since the first harmonic is the dominant Fourier component. However, over deserts as well as some high elevation surfaces the diurnal variation is very large and highly asymmetric so that more frequent measurements are needed to remove the higher order even harmonics [*Oke*, 1978; *Dai and Trenberth*, 2004]. For these surfaces it would be advantageous to have MSU measurements every 6 hours so that all components are eliminated except for multiples of the fourth harmonic. Since such uniformly spaced observations are unavailable, the second harmonic component was estimated by applying the Fourier analysis procedure to the full series of satellite measurements, some of which have different equator crossing times. The equator crossing times also change during a satellites lifetime because of orbital drift, where this variation is also included in the analysis. Using all of this temporal information, *Vinnikov and Grody* [2003] found that it was possible to correct the different MSU observations for diurnal variations up to the second harmonic. Comparisons made between the bias corrections with and without the second harmonic adjustment showed some significant changes (see Table 2). However, the study also found that the second harmonic adjustment only increased the derived global climatic trend from 0.22 K/decade to 0.26 K/decade.

Table 2. Biases of MSU Channel 2 Brightness Temperatures Estimated by Taking Into Account and Ignoring the Second Harmonic Diurnal Variation[a]

Satellite	With Second Harmonic	Ignoring Second Harmonic
TIROS-N	−0.31	−0.03
NOAA-6	0.19	0.21
NOAA-7	−0.27	−0.01
NOAA-8	0.18	0.18
NOAA-9	−0.14	0.03
NOAA-10	0	0
NOAA-11	0.08	0.26
NOAA-12	−0.60	−0.58
NOAA-14	−0.49	−0.34

[a]From *Vinnikov and Grody* [2003]. Units are in kelvins.

[12] Unfortunately, the above cited procedure used to correct for instrumental errors and diurnal variations (up to the second harmonic) is only applicable when the calibration error involves a constant bias for each MSU. As discussed in the next section, we now find that in addition to the constant bias a second calibration adjustment is required due to nonlinear and calibration target errors. This second adjustment includes a brightness and warm target temperature-dependent factor which varies spatially and temporally. Since the temporal variations can have the same periodicities as the diurnal and seasonal variations, the Fourier analysis procedure cannot be used to distinguish between this second calibration adjustment and temperature variations. The second calibration adjustment is determined from the differences between the zonally averaged overlapping satellite measurements at low and high latitudes, after reducing the diurnal variations by averaging the ascending and descending orbital measurements. This removes the first harmonic diurnal component with the second harmonic being the dominant term.

[13] The diurnal variability can be further reduced by only using measurements over the low latitude oceans and high latitude regions such as the Arctic and Antarctic during the summer and winter periods rather than zonally averaged latitudinal bands. However, over high elevated regions such as Antarctica the emissivity variations can result in significant brightness temperature variations for MSU channel 2. Furthermore, the satellite data we use consists of the pentad averaged, 2.5° × 2.5° gridded MSU Channel 2 brightness temperatures. Therefore the spatial variability of emissivity within the grids can lead to errors for high elevation areas when differencing the measurements from overlapping satellites. We have therefore chosen to perform our analysis by averaging the measurements over wide latitudinal bands rather than use the localized regions mentioned above.

[14] While the present study only uses nadir measurements, the reduction in transmittance when viewing off-nadir can be used to significantly reduce the diurnal variations resulting from the surface. Furthermore, since the sources of calibration error are independent of scan position, the off-nadir measurements may provide a more accurate estimate of the calibration adjustments for any viewing angle, including nadir. This of course assumes that

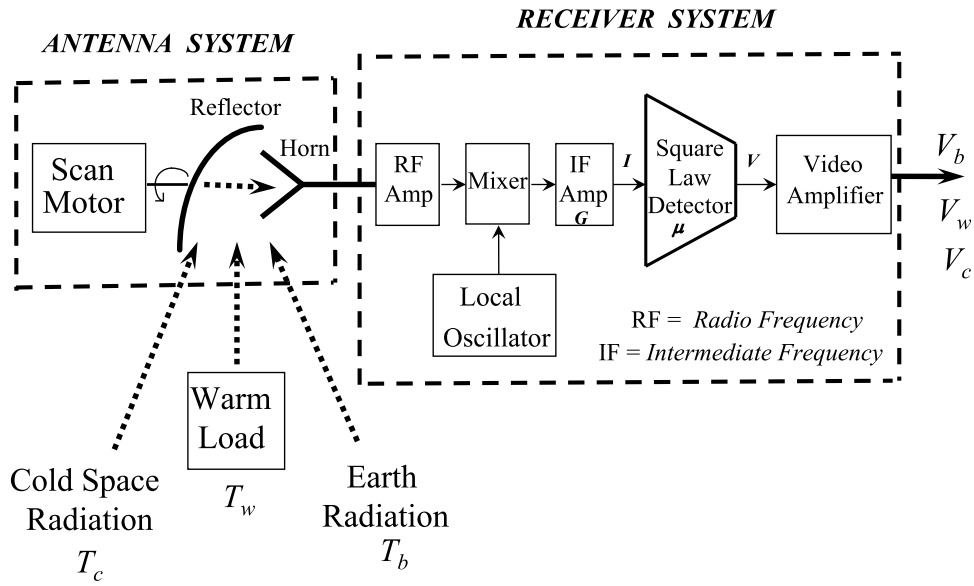

Figure 2. Block diagram of a radiometer showing the antenna and receiver systems. For cross-track scanners such as the MSU the same antenna reflector and feed horn is used to view Earth as well as the two calibration targets. Not shown is the unit which rapidly switches the MSU receiver from the antenna output to a Dicke reference load, while the radiometer output is synchronized to the switching period. The radiometer center frequency and half bandwidth is defined by the local oscillator and IF amplifier, respectively. Errors in the Earth radiation measurement, T_b, result from errors in the cold space, T_c, and warm target, T_w, measurements and uncertainties in the nonlinear parameter, μ.

the higher peaking weighting function at off-nadir viewing does not add any significant stratospheric diurnal variations to the measurements. This approach has not been applied here since it will be shown in section 4 that the removal of the first harmonic diurnal component is sufficient as far as the calibration adjustments are concerned. However, a future study will examine the use of off-nadir measurements for improving the trend analysis.

3. Calibration Uncertainties

[15] A simplified block diagram of a single channel radiometer is shown in Figure 2. The antenna system consists of a scanning reflector and a feed horn that is coupled to the radiometer receiver. As the satellite orbits the Earth, the reflector collects and redirects the Earth's upwelling radiation to the feed horn, while the sensitive receiver detects and amplifies the radiation over a narrow bandwidth centered at the desired frequency of interest.

[16] The radiometer response to the incoming thermal energy is highly linear, so that only two reference measurements are generally required to calibrate the Earth observations. End to end calibration of the radiometer is obtained by having the reflector view cold space and an onboard warm target at the beginning and end of each scan line (see Figure 2). To minimize the errors in calibration accuracy, cross-track scanning radiometers such as the MSU and AMSU utilize the same antenna system to view Earth as well as the two calibration targets. The radiation temperature of cold space is 2.7 K and the physical temperature of the warm target is monitored using platinum resistance thermometers within the target. Interpolation of the Earth observations between these two reference extremes allows the calculation of radiation intensity in terms of an equivalent blackbody, or brightness temperature. This linear calibration equation is given by

$$T_b = I + SV_b \tag{6}$$

where T_b is the input radiation (in brightness temperature units) collected by the radiometer antenna and V_b is the corresponding output voltage, or counts, measured by the instrument. The intercept, I, and slope parameters, S, are obtained from the cold-space and warm load measurements taken as the antenna scans these external targets. These parameters are given by

$$S = \left(\frac{T_W - T_C}{V_W - V_C}\right) \quad , \quad I = T_C - SV_C \tag{7}$$

where V_C and T_C corresponds to the voltage and brightness temperature of the cold space target, while V_W and T_W are the corresponding warm load target values shown in Figure 2. In order to accurately measure small changes in the Earth's brightness temperature, such as that resulting from climate change, one must account for errors in the slope and intercept due to errors in the calibration target measurements.

[17] The brightness temperature of the warm load target is the product of its emissivity ε_{WT} and physical temperature T_{WT} so that $T_W = \varepsilon_{WT} T_{WT}$. Small corrections to T_W denoted as ΔT_W are needed to account for inaccuracies in the warm target temperature (e.g., due to thermal variations within the target), or the fact that the target it is not a perfect blackbody. Similarly, corrections to T_C denoted as ΔT_C are required to account for the uncertain amount of stray radiation entering the antenna sidelobes by active and

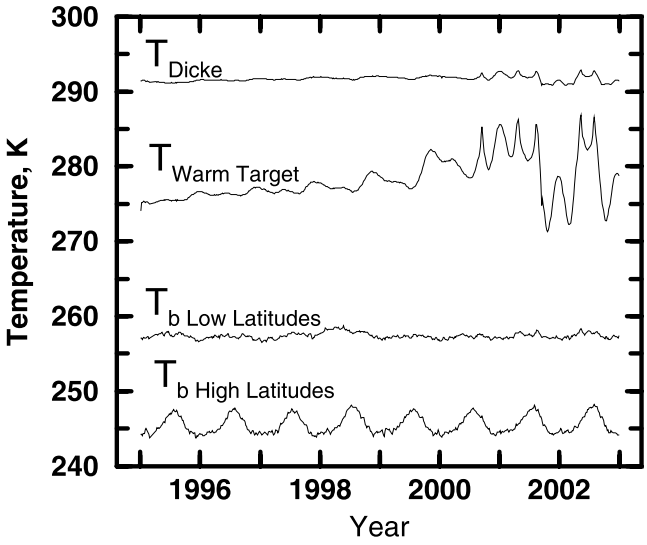

Figure 3. NOAA-14 MSU channel 2 brightness temperature, T_b, Dicke reference temperature, T_{Dicke} and warm target temperature, $T_{\text{Warm Target}}$ during the lifetime of the instrument. The data are averaged globally (85°N–85°S) for low latitudes (30°N–30°S) and high latitudes (remaining part of the globe).

passive sources on board the spacecraft (e.g., S-band transmitters, warm calibration targets) as well as the Earth radiation reflected by the spacecraft. Estimates of the sidelobe effects show that this additional radiation can increase the cold-space measurement by about 2 K for MSU. After adding the corrections ΔT_W and ΔT_C to (7), the additive brightness temperature adjustment to (6) becomes

$$\Delta T_b = K\Delta T_W + (1-K)\Delta T_C, \qquad K = \frac{T_b - T_C}{T_W - T_C}. \tag{8}$$

where the K factor depends on the Earth viewing brightness temperature in addition to the brightness temperature measurements of the warm target and cold space views.

[18] Figure 3 shows the latitudinal and temporal variation of T_b and T_W for the MSU on the NOAA-14 satellite. Also shown is the variation in the Dicke reference load temperature which represents the instrument temperature. The large variations in T_W following 2000 are due to an orbital drift of the satellite, whereas the changes in T_b result almost completely from the periodic seasonal changes in atmospheric temperature. From this plot it is very difficult to detect any cross-talk in T_b due to T_W, i.e., resulting from the calibration errors contained in (8). Any perturbations in T_b due to calibration target error depends on ΔT_W, ΔT_C and the K parameter, whose global average is about 0.85 and varies by ±0.10 between low and high latitudes. Although the correction given by (8) is only approximately constant, *Vinnikov and Grody* [2003] analyzed the globally averaged MSU channel 2 brightness temperatures with the assumption that each instrument differs from each other by a constant bias which is independent of space and time. They then postulated that the differences in the globally averaged brightness temperature for overlapping pairs of satellites are due to the biases and diurnal effects. As mentioned previously, this simple bias adjustment results in the largest global climatic trend estimate of 0.26 K/decade.

[19] In addition to the correction given by (8), prelaunch laboratory measurements reveal a very small nonlinearity in the radiometer response [*Mo et al.*, 2001], which is accurately represented by adding a quadratic term to (6), i.e.,

$$T_b = (I + SV_b) - \mu\, S^2(V_b - V_C)(V_W - V_b). \tag{9}$$

Physically, this nonlinear contribution can be shown to result from an imperfect square law detector or a nonlinear amplifier response. Since there are only two calibration targets available, the nonlinear parameter, μ, is obtained from prelaunch laboratory data [*Mo et al.*, 2001].

[20] To account for errors in the nonlinearity, previous investigators [*Christy et al.*, 2000; *Schabel et al.*, 2003] have added a correction to (9) in the form of $\beta(T_W - T_0)$, and considered a constant instrumental offset, α, so that the calibration correction is

$$\Delta T_b = \alpha + \beta(T_W - T_0) \tag{10}$$

where β is referred to as a nonlinear adjustment parameter and T_0 is the mean warm target temperature. The nonlinear adjustment term is chosen to be a function of the warm target temperature, presumably to account for errors in the instrument-temperature dependence of μ. This target temperature adjustment has been referred to as an "instrument body affect" where the α, β parameters are estimated by minimizing the differences between overlapping satellite measurements using regression analysis with the warm target temperatures as predictands. However, as discussed next, the physical basis of this adjustment is questionable, and is a source of error along with errors associated with the derived parameters.

[21] One of the major difficulties in using empirical corrections, such as (10), is that inaccuracies in both the model and adjustment parameters can produce errors in the corrected measurements. To illustrate this problem, Figure 3 shows how the drifts in the satellite orbit can generate trend-like variations in the target temperature that are not related to climate change. These variations in T_w can artificially suppress the climatic temperature trend in the measurements due to errors in the model as well as the derived β parameters. For example, the globally averaged trend attains a maximum value of 0.26 K/10 yr without any target temperature corrections [*Vinnikov and Grody*, 2003; C. A. Mears, private communication, 2004], while the trend decreases to 0.13 K/10 yr [*Mears et al.*, 2003] and 0.05 K/10 yr [*Christy et al.*, 2003] after applying the target temperature adjustment. *Mears et al.* [2003] suggests that the differences in trend when using (10) are mainly due to the larger β parameter derived for the NOAA-9 satellite by *Christy et al.* [2003]. Although all investigators conclude that the accuracy of the climatic trend depends on the adjustment parameters, we also believe that the trend depends on the statistical method used to derive the adjustment parameters as well as the accuracy of the calibration adjustment model itself.

[22] To examine the physical basis of (10), Figure 3 displays the temporal variations of the globally averaged internal (Dicke) temperature in addition to the external

(warm target) temperature for the NOAA-14 satellite. Heat balance of a satellite depends on the equator crossing time of its orbit. From the beginning of 1995 to the end of 2002 the equator crossing time for ascending orbits of this satellite has changed by almost 5 hours, from 13:40 to 18:30. Consequently, the external warm load target temperature changed by 15 K. At the same time, the instrument temperature, which corresponds to the Dicke reference load temperature, remained stable in the range ±1 K. Laboratory test data show that such variations are too small to cause noticeable variations in the nonlinearity coefficients [*Mo et al.*, 2001]. The hypothetical adjustment given by (10) was therefore rejected by *Vinnikov and Grody* [2003]. Although the temperature dependence of the nonlinearity is small, there is still a possibility that each MSU instrument has a bias in the nonlinearity coefficient. In our analysis we account for errors in the nonlinear parameter using a physically based correction.

[23] Recognizing that the calibration is nearly linear, (9) can be written as

$$T_b = (I + SV_b) - \mu(T_b - T_C)(T_W - T_b) \tag{11}$$

where the correction for errors in the calibration targets was given by (8) while the nonlinear correction is $-(T_b - T_C)(T_W - T_b)\Delta\mu$ where $\Delta\mu$ is the nonlinear bias. Therefore the calibration equation can be rewritten as,

$$T_b = T_b'' + [K\Delta T_W + (1 - K)\Delta T_C - Z\Delta\mu] \tag{12a}$$

where

$$Z = (T_b - T_C)(T_W - T_b) \tag{12b}$$

and

$$K = \frac{T_b - T_C}{T_W - T_C}. \tag{12c}$$

Equation (12a) contains the error-free measurement, T_b'', together with a bracketed term that represents the instrumental bias. The bias contains corrections for the nonlinear parameter, $\Delta\mu$, cold-space, ΔT_C, and warm target, ΔT_W. Since all of these corrections are multiplied by the K and Z factors, the bias is not constant but varies with latitude and time. However, since both K and Z depend on T_b, they are highly correlated. This is shown in Figure 4 by plotting K against Z for the MSU on NOAA-14. The data were obtained for the full time period (see Figure 3) where each point is the globally average value over 10o latitude bands. Applying a linear regression to the data, we obtain the equation,

$$K = a - bZ \tag{13}$$

where $a = 1.016$ and $b = 1.750 \times 10^{-5}$. Equation (13) fits the data with a correlation coefficient of 0.995, where the scatter of points about the straight line (shown in Figure 4) is mostly due to variations in T_W. The equation can also be obtained from (12b) and (12c) by recognizing that $K(1 - K) = Z/(T_W - T_C)^2$. After linearizing this equation using a Taylor expansion about $K = 0.85$, and setting T_W to a mean value of 280 K, we obtain (13) with nearly the same coefficients.

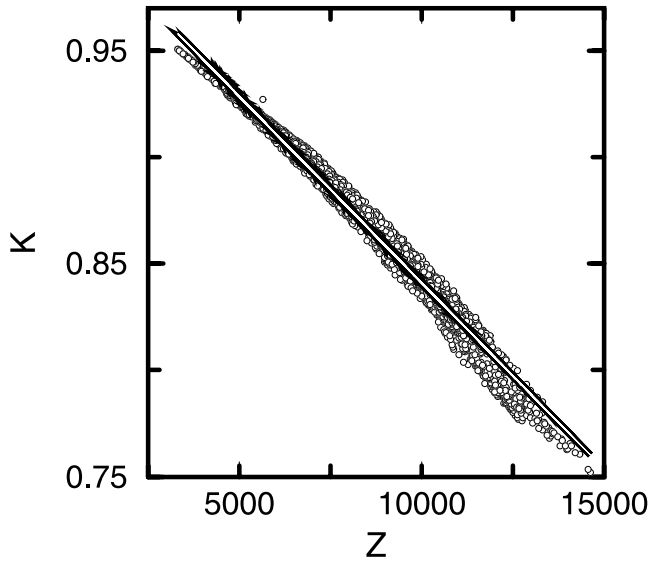

Figure 4. NOAA-14 MSU channel 2 calibration factors, K and Z plotted against one another from the global (85°N–85°S) data. Each data point represents the globally averaged measurements over a 10° latitude band. Also shown is the straight line fit to the data given by equation (13).

[24] Substituting (13) into (12a), we obtain the final result,

$$T_b = T_b'' + [\delta T - Z\delta U] \tag{14a}$$

where

$$\delta T = \Delta T_C + a(\Delta T_W - \Delta T_C) \tag{14b}$$

and

$$\delta U = \Delta\mu + b(\Delta T_W - \Delta T_C). \tag{14c}$$

so that the bracketed correction term in (14a), which represents the instrumental bias, now only contains two free parameters, δT and δU. The first parameter, δT, is the calibration offset which depends on the errors in the two calibration targets. The second parameter, δU, depends on the nonlinear and calibration target errors, which are multiplied by the Z factor that varies is space and time. It is implicitly assumed throughout this paper that the parameters δT and δU in (14a) are constant, independent of time, during the life of a given instrument. This implies that the sidelobe contributions contributing to the cold-space uncertainty remain constant, that the warm target emissivity and its temperature error are constant, and that the nonlinearity associated with the detector element and amplifiers remains constant throughout the instruments lifetime. However, any significant changes in these parameters during the satellite overlap periods should degrade the accuracy of the resulting adjustments obtained when using (14a). Therefore, as an indirect verification of the assumed stability of δT and δU, in section 4 we compare

the long-term differences between overlapping satellite instruments for the corrected against uncorrected MSU measurements.

[25] In an earlier analysis by *Vinnikov and Grody* [2003], a procedure was developed to only determine constant calibration bias adjustments such as δT. In that study the differences in the globally averaged brightness temperature for overlapping observations of pairs of satellites were used to determine the constant biases of each instrument as well as the effects of diurnal variations on the different satellite measurements. We shall now determine both the δT and δU parameters by minimizing the differences between overlapping satellite measurements using statistical analysis with the Z-factors being the predictands. The overlapping pentads of satellite measurements listed in Table 4 can be used individually to obtain a multitude of equations for determining the parameters. However, the nadir viewing satellite measurements used here view the same location on Earth at different times. This spatial variability introduces random noise-like variations in the overlapping measurements, which can affect the accuracy of the derived calibration parameters. To reduce this noise, the measurements are grouped [*Wald*, 1940] into two broad latitudinal bands, L, joined at common latitude, and temporally averaged over an extended time period, t_S, comprising many pentads. The long-time average is equally important for reducing the effects of any trends in T_W on the analysis. Equation (14a) then becomes

$$\langle T_{L,S}\rangle_{t_S} = \langle T''_{L,S}\rangle_{t_S} + \left[\delta T_S - \langle Z_{L,S}\rangle_{t_S}\delta U_S\right], \tag{15}$$

where the operator $\langle\rangle$ denotes the fact that the measurements and Z-factors for each satellite instrument, S, are spatially and temporally averaged, where $T_{L,S}$ is the brightness temperature, $T''_{L,S}$ is the error-free measurement and $Z_{L,S}$ is the factor defined by (12b). Furthermore, as discussed previously, the diurnal variation between the overlapping measurements is reduced by averaging the ascending and descending orbital data. We therefore neglect any differences in the error-free measurements from two satellites $S = S1$ and $S = S2$ when zonally averaged over the same time period $t_{S1\text{-}S2}$ so that

$$\langle T_{L,S1}\rangle_{t_{S1-S2}} - \langle T_{L,S2}\rangle_{t_{S1-S2}} = (\delta T_{S1} - \delta T_{S2}) - \langle Z_{L,S1}\rangle_{t_{S1-S2}}\delta U_{S1} + \langle Z_{L,S2}\rangle_{t_{S1-S2}}\delta U_{S2}, \tag{16}$$

where the above equation assumes that the differences in the space-time averaged brightness temperature between overlapping satellite instruments is due to calibration error. An algorithm is formulated next based on this equation to adjust all of the MSUs for the calibration targets and nonlinear errors.

[26] A least squares optimization technique is used to obtain the parameters by minimizing the difference in the zonally averaged brightness temperature for the different latitude bands. As discussed in section 4, the simplest solution is obtained when the calibration of at least one of the instruments is known perfectly, so that calibration parameters for all other MSUs can be referenced to that sensor. Unfortunately, we have no way of knowing the calibration accuracy of any MSU, particularly after the instruments have been launched. As such, only the offset, δT, can be referenced to an arbitrary instrument (e.g., NOAA-10 MSU) since the referenced offset adds the same constant to all MSU measurements, thereby unaffecting the use of the data for climatic trend analysis. However, a change in the δU parameter for one MSU changes the bias parameters for all other instruments non-uniformly. Therefore an incorrect reference for δU can significantly alter the trend of the MSU time series so that the best estimates of this parameter must be obtained for each instrument using the minimization approach described next.

4. Calibration Algorithm

[27] Differences between the brightness temperatures from overlapping MSU observations are used to determine the calibration parameters contained in (16). These differences vary both spatially and temporally, where both variations are used in developing the retrieval algorithm. While more than two latitudinal bands can be used in the analysis, we found it sufficient to only consider two equal area latitudinal belts. These regions were referred to in Figure 3 and are denoted as $L = l$ for the low latitudes (30°N–30°S) and $L = h$ for the remaining part of the globe which extends to a latitude of 85° in both hemispheres.

[28] The satellite data consist of the warm target temperatures and pentad averaged, 2.5° × 2.5° gridded MSU Channel 2 brightness temperatures closest to the nadir (nadir ±1) beam position for both the ascending and descending orbits of all 9 satellites [*Vinnikov and Grody*, 2003]. Table 4 lists the number of overlapping pentad observations for the different satellites. As an example of this data, Figure 5 displays the complete time series of the spatially averaged NOAA-12 and NOAA-14 MSU measurements (top) and Z-factors (bottom), for the two latitude belts. The diurnal variations are reduced by averaging the ascending and descending measurements for each pentad so that much of the temporal variations of the brightness temperature results from seasonal changes while the warm target temperature varies mainly due to the orbital drift of the satellites. Both the measurements and Z-factors show different temporal and spatial variations for the two satellites during the 1995 and 1999 overlap period. However, it is difficult to observe any cross-talk between the brightness temperature measurements and Z-factors. Also not evident is the small bias between instruments, and the fact that the bias in the brightness temperature is slightly different for the two latitude zones. As discussed later, the high latitude bias is 0.19 K while it is only 0.05 K at low latitudes between these two satellites (see Table 4). In retrospect, it is should be noted that the latitudinal variation in the bias between MSUs is what started our investigation of calibration errors, leading eventually to (15). Equation (15) is also quite different than the empirical adjustment (10), which only contains the warm target temperature. As such, (10) cannot accurately account for the latitudinal variation of the bias, and can therefore lead to errors when determining the latitudinal distribution of the temperature trend.

[29] The spatial and temporal variations shown in Figure 5 are however insufficient for determining the calibration

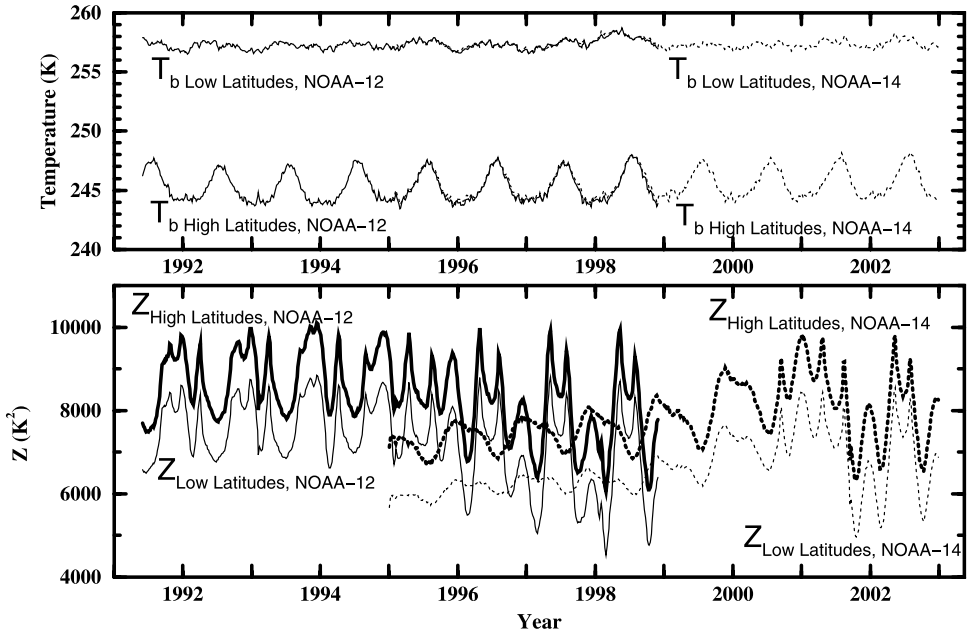

Figure 5. (top) Averaged brightness temperatures for NOAA-12 (1991–1999) and NOAA-14 satellite (1995–2003) instruments for two latitude regions. (bottom) Also shown are the corresponding *Z*-factors.

adjustments for the two satellite instruments. In fact, a minimum of three overlapping satellite measurements is needed to derive the calibration adjustments when using two latitude bands. This can be seen by applying (16) to three satellites (*S*1, *S*2, *S*3) and two latitude bands ($L = l, h$), and expressing the 6 equations in matrix form, namely,

$$\begin{bmatrix} \Delta T_{h,S1-S2} \\ \Delta T_{l,S1-S2} \\ \Delta T_{h,S2-S3} \\ \Delta T_{l,S2-S3} \\ \Delta T_{h,S1-S3} \\ \Delta T_{l,S1-S3} \end{bmatrix} = \begin{bmatrix} 1 & 0 & 0 & -\langle Z_{h,S1}\rangle_{t_{S1-S2}} & \langle Z_{h,S2}\rangle_{t_{S1-S2}} & 0 \\ 1 & 0 & 0 & -\langle Z_{l,S1}\rangle_{t_{S1-S2}} & \langle Z_{l,S2}\rangle_{t_{S1-S2}} & 0 \\ 0 & 1 & 0 & 0 & -\langle Z_{h,S2}\rangle_{t_{S2-S3}} & \langle Z_{h,S3}\rangle_{t_{S2-S3}} \\ 0 & 1 & 0 & 0 & -\langle Z_{l,S2}\rangle_{t_{S2-S3}} & \langle Z_{l,S3}\rangle_{t_{S2-S3}} \\ 0 & 0 & 1 & -\langle Z_{h,S1}\rangle_{t_{S1-S3}} & 0 & \langle Z_{h,S3}\rangle_{t_{S1-S3}} \\ 0 & 0 & 1 & -\langle Z_{l,S1}\rangle_{t_{S1-S3}} & 0 & \langle Z_{l,S3}\rangle_{t_{S1-S3}} \end{bmatrix} \cdot \begin{bmatrix} \delta T_{S1-S2} \\ \delta T_{S2-S3} \\ \delta T_{S1-S3} \\ \delta U_{S1} \\ \delta U_{S2} \\ \delta U_{S3} \end{bmatrix} \tag{17}$$

The left-most column matrix contains the differences between the measurements, which are temporally averaged over the three satellite overlap periods ($t_{S1\text{-}S2}$, $t_{S2\text{-}S3}$, $t_{S1\text{-}S3}$) and spatially averaged over the two latitude zones, i.e.,

$$\Delta T_{h,S1-S2} \equiv \langle T_{h,S1}\rangle_{t_{S1-S2}} - \langle T_{h,S2}\rangle_{t_{S1-S2}}, \quad \text{etc.,} \tag{18a}$$

while the right-most column matrix contains the nonlinear adjustments and differences in the calibration offset defined as

$$\delta T_{S1-S2} \equiv \delta T_{S1} - \delta T_{S2}, \ \text{etc.,} \tag{18b}$$

However, $\delta T_{S1\text{-}S2} + \delta T_{S2\text{-}S3} = \delta T_{S1\text{-}S3}$ so that the three elements are dependent. The element $\delta T_{S1\text{-}S3}$ is therefore removed from (17) so that the equation becomes;

$$\begin{bmatrix} \Delta T_{h,S1-S2} \\ \Delta T_{l,S1-S2} \\ \Delta T_{h,S2-S3} \\ \Delta T_{l,S2-S3} \\ \Delta T_{h,S1-S3} \\ \Delta T_{l,S1-S3} \end{bmatrix} = \begin{bmatrix} 1 & 0 & -\langle Z_{h,S1}\rangle_{t_{S1-S2}} & \langle Z_{h,S2}\rangle_{t_{S1-S2}} & 0 \\ 1 & 0 & -\langle Z_{l,S1}\rangle_{t_{S1-S2}} & \langle Z_{l,S2}\rangle_{t_{S1-S2}} & 0 \\ 0 & 1 & 0 & -\langle Z_{h,S2}\rangle_{t_{S2-S3}} & \langle Z_{h,S3}\rangle_{t_{S2-S3}} \\ 0 & 1 & 0 & -\langle Z_{l,S2}\rangle_{t_{S2-S3}} & \langle Z_{l,S3}\rangle_{t_{S2-S3}} \\ 1 & 1 & -\langle Z_{h,S1}\rangle_{t_{S1-S3}} & 0 & \langle Z_{h,S3}\rangle_{t_{S1-S3}} \\ 1 & 1 & -\langle Z_{l,S1}\rangle_{t_{S1-S3}} & 0 & \langle Z_{l,S3}\rangle_{t_{S1-S3}} \end{bmatrix} \cdot \begin{bmatrix} \delta T_{S1-S2} \\ \delta T_{S2-S3} \\ \delta U_{S1} \\ \delta U_{S2} \\ \delta U_{S3} \end{bmatrix} \tag{19}$$

To formulate the solution, (19) is rewritten using matrix notation

$$\mathbf{\Delta} T_{\mathbf{M}} = \mathbf{Z}_{\mathbf{M,N}} \cdot \mathbf{\delta X}_{\mathbf{N}} \tag{20}$$

where $\mathbf{\delta X_N}$ is a column matrix of dimension $\mathbf{N} = 5$, which contains the calibration adjustments for each overlapping MSU. Similarly, $\mathbf{\Delta T_M}$ is a column matrix of dimension $\mathbf{M} = 6$, which contains the overlapping measurements for each latitude band. The rectangular matrix $\mathbf{Z_{M,N}}$ contains the Z-factors for all of the overlapping satellites and has the dimensions $\mathbf{MxN} = 6 \times 5$.

[30] Since the *Z*-matrix is rectangular, where $\mathbf{M} > \mathbf{N}$, equation (20) represents an over determined system of equations for the calibration parameters. The least squares solution is formally obtained by first multiplying each left side of (20) by the transpose of the $\mathbf{Z_{M,N}}$ matrix. The square

matrix formed by the product of Z-matrices is then inverted to obtain the solution [e.g., *Gelb*, 1974], i.e.,

$$\delta \mathbf{X_N} = \mathbf{A_{N,M}} \cdot \mathbf{\Delta T_M}, \tag{21a}$$

with

$$\mathbf{A_{N,M}} = \left[\mathbf{Z^t_{M,N}} \cdot \mathbf{Z_{M,N}}\right]^{-1} \cdot \mathbf{Z^t_{M,N}} \tag{21b}$$

where $\mathbf{A_{N,M}}$ is the pseudoinverse where "t" is the transpose and "-1" is the inverse operator. For the pseudoinverse matrix to exist the *Z*-factors in $\mathbf{Z_{M,N}}$ must be independent of each other. This also implies that the measurements are independent so that

$$\Delta T_{h,S1-S2} + \Delta T_{h,S2-S3} \neq \Delta T_{h,S1-S3} \tag{22a}$$

and

$$\Delta T_{l,S1-S2} + \Delta T_{l,S2-S3} \neq \Delta T_{l,S1-S3}. \tag{22b}$$

To satisfy this condition, $t_{S1\text{-}S2}$, $t_{S2\text{-}S3}$ and $t_{S1\text{-}S3}$ must be different from one another so that the period of observation for satellites 1 and 3 extends beyond that of the center-most satellite, 2. Furthermore, the set of three overlapping measurements must form a closed system so that satellite 3 overlaps satellite 1 in addition to satellite 2. This closed loop configuration is denoted as (1-2-3-1) and is a necessary condition in order to obtain closure among the equations. While there are 12 different overlaps among the 9 satellites, only 5 closed loops are formed (see Table 4). These closed loop sequences are (6, 7, 8, 6), (5, 2, 3, 5), (5, 3, 4, 5), (7, 8, 9, 7), and (5, 2, 3, 4, 5) where the integers 1 through 9 correspond to the TIROS-N, NOAA-6, -7, -8, -9, -10, -11, -12, and NOAA-14 satellites, respectively. However, it is important to note that the closed loop condition is only necessary to initialize the procedure by determining the calibration adjustments for 3 of the 9 satellites. The calibration adjustments for the remaining MSU instruments can be obtained through connections with other satellites that overlap those in the closed loop. As such, a solution can be obtained using as a minimum of 9 overlapping satellites, 3 of which form a closed loop so that $\mathbf{M} = 9 \times 2 = 18$ and $\mathbf{N} = 9 \times 2 - 1 = 17$.

[31] To obtain a consistent set of calibration adjustments, all 12 overlapping satellites measurements are used in forming the solution. The equation is again expressed in matrix form where the dimension of the matrices in (20) now increases since $\mathbf{M} = 12 \times 2 = 24$. The solution is again given by (21) where all of the calibration offsets are referenced to the NOAA-10 instrument, i.e., $\delta T_{NOAA\text{-}10} = 0$. This approach of utilizing all of the overlapping measurements improves the accuracy of the results by making sure that the adjustments minimize the differences between all 12 interconnecting satellite measurements, of which there are 5 closed loops around 3 or 4 instruments.

[32] As part of our investigation, we also considered the use of three latitudinal bands (equatorial, midlatitude, polar) rather than the two bands mentioned above. However, the measurements from the three bands were highly correlated so that we still found it necessary to incorporate the closed loop condition referred to above. The closed loop condition is required because none of the satellite instruments are used as a reference with regard to the δU parameter. To show this, we consider one of the instruments, S1, to be perfectly calibrated with no uncertainties so that $\delta U_{S1} = 0$. Equation (19) is then reduced to

$$\begin{bmatrix} \Delta T_{h,S1-S2} \\ \Delta T_{l,S1-S2} \\ \Delta T_{h,S2-S3} \\ \Delta T_{l,S2-S3} \\ \Delta T_{h,S1-S3} \\ \Delta T_{l,S1-S3} \end{bmatrix} = \begin{bmatrix} 1 & 0 & \langle Z_{h,S2}\rangle_{t_{S1-S2}} & 0 \\ 1 & 0 & \langle Z_{l,S2}\rangle_{t_{S1-S2}} & 0 \\ 0 & 1 & -\langle Z_{h,S2}\rangle_{t_{S2-S3}} & \langle Z_{h,S3}\rangle_{t_{S2-S3}} \\ 0 & 1 & -\langle Z_{l,S2}\rangle_{t_{S2-S3}} & \langle Z_{l,S3}\rangle_{t_{S2-S3}} \\ 1 & 1 & 0 & \langle Z_{h,S3}\rangle_{t_{S1-S3}} \\ 1 & 1 & 0 & \langle Z_{l,S3}\rangle_{t_{S1-S3}} \end{bmatrix} \begin{bmatrix} \delta T_{S1-S2} \\ \delta T_{S2-S3} \\ \delta U_{S2} \\ \delta U_{S3} \end{bmatrix} \tag{23}$$

This is an overdetermined system of equations for the four calibration parameters whose solution is again given by (21a) and (21b), where the pseudoinverse matrix exists as long as the Z-elements for two latitude bands are different at the time intervals $t_{S1\text{-}S2}$ and $t_{S2\text{-}S3}$ for example. Furthermore, by removing two of the six measurements (e.g., $\Delta T_{h,S2\text{-}S3}$, $\Delta T_{l,S2\text{-}S3}$) a deterministic solution is obtained, namely,

$$\begin{bmatrix} \Delta T_{h,S1-S2} \\ \Delta T_{l,S1-S2} \\ \Delta T_{h,S1-S3} \\ \Delta T_{l,S1-S3} \end{bmatrix} = \begin{bmatrix} 1 & 0 & \langle Z_{h,S2}\rangle_{t_{S1-S2}} & 0 \\ 1 & 0 & \langle Z_{l,S2}\rangle_{t_{S1-S2}} & 0 \\ 1 & 1 & 0 & \langle Z_{h,S3}\rangle_{t_{S1-S3}} \\ 1 & 1 & 0 & \langle Z_{l,S3}\rangle_{t_{S1-S3}} \end{bmatrix} \begin{bmatrix} \delta T_{S1-S2} \\ \delta T_{S2-S3} \\ \delta U_{S2} \\ \delta U_{S3} \end{bmatrix} \tag{24}$$

The advantage of this approach is that the calibration adjustments can be obtained without the need for any closed loops between overlapping satellites. This also reduces the minimum number of satellite overlaps from 9 to 8, which is one less than the total number of satellites. However, since the adjustments and corresponding climatic trend vary depending on which instrument is used as a reference, this approach is not considered at this time. This technique is, however, used to estimate the uncertainty in the adjustments and corresponding climatic trends by comparing the results using different MSU instruments as reference (K. Y. Vinnikov et al., Observed and model-simulated air temperature trend at the surface and troposphere, submitted to *Nature*, 2004) (hereinafter referred to as Vinnikov et al., submitted manuscript, 2004).

5. Calibration Adjustments

[33] The calibration adjustments obtained using only $\delta T_{NOAA\text{-}10} = 0$ are listed in Table 3 along with the RMS errors for each MSU. It is noted that the δT_S adjustments are less than 0.5 K, with RMS errors around 0.05 K. Also, the δU_S adjustments which correct for the latitudinal variation of the bias are of the same magnitude as the nonlinearity parameters [*Mo et al.*, 2001] with errors that are an order of magnitude smaller. Furthermore, since the *Z*-factor varies by about ± 5000 K^2, the brightness temperature corrections due to δU_S and δT_S are comparable in magnitude. To check the quality of the adjustments, Table 4 shows the differences in brightness temperature between the high latitude and low latitude bands before and after making the calibration adjustments. The differences after making the calibration adjustments are very small, with none of them exceeding 0.02 *K*. It is therefore concluded that the adjustments are

Table 3. Calibration Parameters, δT_S, δU_S and Corresponding Root Mean Square Errors (RMSE) Obtained Using 2 Latitude Regions and the 12 Overlapping Satellites[a]

Satellite, S	δT_S, K	RMSE, K	δU_S, $\times 10^{-4}$, K^{-1}	RMSE, $\times 10^{-4}$, K^{-1}
TIROS-N	0.14	0.06	−0.35	0.09
NOAA-6	0.09	0.05	−0.07	0.06
NOAA-7	0.09	0.05	−0.45	0.05
NOAA-8	−0.07	0.05	−0.40	0.07
NOAA-9	−0.40	0.04	−1.21	0.06
NOAA-10	0	0	−0.53	0.07
NOAA-11	−0.46	0.03	−0.94	0.07
NOAA-12	0.30	0.04	−0.18	0.08
NOAA-14	0.06	0.04	−0.77	0.09

[a]All offset adjustments are referenced to the NOAA-10 instrument, which is considered to have no adjustment, i.e., $\delta T_{NOAA\text{-}10} = 0$.

almost perfect; eliminating any differences between high and low latitudes. These very small differences also suggest that the adjustment for diurnal variations is sufficient and that the calibration parameters are essentially constant during the satellite overlap periods, some of which extended beyond three years. It should be understood, however, that the corrections listed in Table 3 are based on the MSU measurements supplied to us by NOAA, which contains "corrections" to the NOAA 12 nonlinear coefficients based on the paper by *Mo* [1995]. Obviously, the adjustments listed in Table 3 would be different if, for example, the MSU was calibrated using the "incorrect" set of nonlinear coefficients or if in fact no nonlinearity was applied. To check the robustness of the procedure, we ran the algorithm using measurements which contained the "incorrect" nonlinear coefficients for NOAA 12. It was then found that the largest changes in the calibration adjustments occurred for the δU_S parameter for NOAA 12, with almost no change to the other parameters in Table 3. Also, after the adjustments were applied, the differences between satellite measurements were reduced to the same small values given in Table 4.

6. Summary

[34] The 25 years of MSU satellite measurements provide a unique data set to estimate the long-term, global climatic change of atmospheric temperature. To homogenize the data, the measurements from all MSUs must be adjusted for their different observation times and intercalibrated to account for instrumental differences. In order to accurately account for instrumental errors a newly developed calibration equation is obtained that contains adjustments due to errors in the two calibration targets and nonlinearity parameter. The calibration adjustment is given by (14a) and has the two terms (14b) and (14c). The first term δT is a constant offset that physically results from errors in the cold-space and warm target measurements. The second term δU results from the same errors in the two target measurements together with the error in the instruments nonlinear parameter. However, unlike the offset, this second term is multiplied by a Z factor that is a function of the brightness temperature measurement, and therefore produces temporal and latitudinal variations in the MSU bias. Since the Z-factor varies differently in space and time depending on the satellite (see Figure 5), the calibration adjustments, δT and δU are determined using differences in the overlapping MSU measurements at two widely separated latitude bands. However, to obtain a solution it is necessary that some of the overlaps form closed loops so that, for example, the period of observations for satellites 1, 2, and 3 not only overlap each other but satellite 3 overlaps satellite 2 in addition to satellite 1. Interestingly, this closed loop condition occurs because none of the satellite instruments can be used as a reference with regard to δU. If, however, δU is known a priori for one MSU, the adjustments for all the other instruments can be obtained without the need for any closed loops.

[35] To apply the adjustment procedure, it is necessary to minimize any differences between the overlapping measurements that arise from diurnal temperature variations. These diurnal variations are reduced by averaging the ascending and descending satellite measurements. The technique removes all odd harmonic components, although errors are possible due to the remaining even harmonics. To test the procedure, the difference between overlapping MSU measurements are compared as a function of latitude. As shown in Table 4, the difference between measurements at low and high latitude bands were initially large for some satellites, while the adjusted

Table 4. Difference Between Satellites Measurements (s, k) for the High, $\Delta T_{h,s-k}$, and Low, $\Delta T_{l,s-k}$, Latitudinal Belts Before and After Applying the Calibration Adjustments Listed in Table 3[a]

			Unadjusted Calibration, K			Adjusted Calibration, K		
Satellite - s -	Satellite - k -	Overlap Pentads	High Latitude $\Delta T_{h,s-k}$	Low Latitude $\Delta T_{l,s-k}$	High − Low Latitude $\Delta T_{h,s-k} - \Delta T_{l,s-k}$	High Latitude $\Delta T_{h,s-k}$	Low Latitude $\Delta T_{l,s-k}$	High − Low Latitude $\Delta T_{h,s-k} - \Delta T_{l,s-k}$
N-6	T-N	41	−0.24	−0.17	−0.07	0.00	0.00	0.00
N-7	N-6	99	0.26	0.15	0.11	0.00	0.00	0.01
N-8	N-7	79	−0.17	−0.17	−0.00	0.00	−0.01	0.01
N-9	N-6	73	0.29	0.01	0.28	0.00	0.01	−0.01
N-9	N-7	6	−0.05	−0.24	0.20	0.00	0.01	−0.01
N-9	N-8	13	0.12	−0.06	0.19	0.00	−0.01	0.01
N-10	N-9	18	−0.03	0.16	−0.19	0.00	0.00	0.00
N-11	N-10	213	−0.23	−0.34	0.11	0.01	0.01	0.01
N-12	N-10	19	0.01	0.11	−0.09	0.02	−0.00	−0.02
N-12	N-11	316	0.18	0.39	−0.21	0.02	0.03	−0.02
N-14	N-11	55	0.30	0.33	−0.03	0.01	−0.02	0.01
N-14	N-12	280	0.19	0.05	0.14	0.01	0.02	−0.01

[a]Also shown are the corresponding differences $\Delta T_{h,s\text{-}k} - \Delta T_{l,s\text{-}k}$ as well as the number of overlapping pentads between different satellites, s and k.

measurements show insignificant differences between the MSUs for both latitude bands. We therefore concluded that any further improvements in the diurnal corrections are unnecessary as far as the calibration adjustment issue is concerned. Furthermore, the initial assumption that δT and δU are constant over the overlap period between satellites appears to be justified by the very small differences in the adjusted measurements.

[36] This study reports our latest findings concerning the MSU calibration. However, of major importance is the effect of these new calibration adjustments on the derived global climatic trend. In our first investigation [*Vinnikov and Grody*, 2003] where only a constant bias was applied to the measurements, the global trend increased from 0.22 K/decade to 0.26 K/decade when a second harmonic diurnal adjustment was included in the determination of the bias and trend. However, the application of these new calibration adjustments with no second-harmonic adjustments results in a global trend with nearly the same 0.17 K/decade obtained from surface observations (Vinnikov et al., submitted manuscript, 2004).

Appendix A: Emissivity Effect on Brightness Temperature Change

[37] Changes in surface emissivity can introduce brightness temperature changes which can be misinterpreted as due to temperature. Equation (1) is used to determine the brightness temperature change due to changes in emissivity. Since the effect of emissivity change on brightness temperature does not vary much for different temperature profiles, it is sufficient to consider an isothermal atmosphere (i.e., $T_d = T_u = T_S\,(1 - \tau_S)$ so that (1) becomes

$$T_b = T_S\left[1 - \tau_S^2(1 - \varepsilon_S)\right]. \tag{A1}$$

Therefore the change in the globally averaged brightness temperature ΔT_b to a change in emissivity $\Delta\varepsilon_S$ is

$$\Delta T_b = \tau_S^2 T_S \Delta\varepsilon_S. \tag{A2}$$

Unlike the effect of diurnal temperature change given by (5), the changes due to emissivity depend on the transmittance-squared which results in a smaller effect than the diurnal variations. This smaller emissivity effect occurs because of the compensating changes in the surface radiation and reflected downwelling radiation terms in (1). However, over high elevation regions, the decreased surface pressure reduces the transmittance (see (2)) and increases the emissivity effect on brightness temperature. Therefore one cannot ignore the emissivity variation of ice when performing analysis over regions such as Antarctica. Fortunately, however, the emissivity effects are quite small for global analysis.

[38] To evaluate the global effects of emissivity change on brightness temperature, we consider the effect of decreasing sea ice concentration. For the MSU channels the emissivity over land is about the same as new sea ice ($\varepsilon_0 \cong 0.95$), whereas the oceans have the lowest emissivity ($\varepsilon_w \cong 0.50$). Considering that the globally averaged emissivity varies due to changing sea ice concentration, Δf_{ice}, then $\Delta\varepsilon_S = (\varepsilon_0 - \varepsilon_w)\Delta f_{ice}$ and from (A2) we obtain

$$\Delta T_b = \tau_S^2 T_S(\varepsilon_o - \varepsilon_w) \cdot \Delta f_{ice}. \tag{A3}$$

Over the past 30 years the sea ice in the northern hemisphere has been reduced from 12.2×10^6 km^2 to 11.2×10^6 km^2 [*Cavalieri et al.*, 2003]. Since the total area of the Earth is 510×10^6 km^2, $\Delta f_{ice} = 1/510$ so that from (A3) we obtain $\Delta T_b \cong 0.003$ K for MSU channel 2. This brightness temperature change is negligible due to the small value of Δf_{ice}. However, larger values of Δf_{ice} would obviously occur if the region under consideration was not global but confined only to high latitudes [*Swanson*, 2003].

[39] **Acknowledgments.** Sponsored by NOAA grants COMM NA17EC1483 and NA06GPO403. The views expressed in this publication are those of the authors and do not necessarily represent those of NOAA. The authors would like to express their gratitude to Alan Robock, Changyong Cho, and Jim Yoe for their constructive criticism and suggestions in improving the clarity of the paper.

References

Cavalieri, D. J., C. L. Parkinson, and K. Y. Vinnikov (2003), Thirty-year satellite record reveals contrasting Arctic and Antarctic decadal sea ice variability, *Geophys. Res. Lett.*, *30*(18), 1970, doi:10.1029/2003GL018031.

Christy, J. R., R. W. Spencer, and W. D. Braswell (2000), MSU tropospheric temperatures: Dataset construction and radiosonde comparisons, *J. Atmos. Oceanic Technol.*, *17*, 1153–1170.

Christy, J. R., R. W. Spencer, W. B. Norris, W. D. Braswell, and D. E. Parker (2003), Error estimates of version 5 of MSU-AMSU bulk atmospheric temperatures, *J. Atmos. Oceanic Technol.*, *20*, 613–629.

Dai, A., and K. E. Trenberth (2004), The diurnal cycle and its depiction in the Community Climate System Model, *J. Clim.*, *17*, 930–951.

Gelb, A. (1974), *Applied Optimal Estimation*, p. 19, MIT Press, Cambridge, Mass.

Grody, N. C. (1993), Remote sensing of the atmosphere from satellites using microwave radiometry, in *Atmospheric Remote Sensing by Microwave Radiometry*, edited by M. A. Janssen, John Wiley, Hoboken, N. J.

Janssen, M. A. (1993), An introduction to the passive microwave remote sensing of atmospheres, in *Atmospheric Remote Sensing by Microwave Radiometry*, edited by M. A. Janssen, John Wiley, Hoboken, N. J.

Mears, C. A., M. C. Schabel, and F. J. Wentz (2003), A reanalysis of the MSU Channel 2 tropospheric temperature record, *J. Clim.*, *16*, 3650–3664.

Mo, T. (1995), A study of the Microwave Sounding Unit on the NOAA-12 satellite, *IEEE Trans. Geosci. Remote Sens.*, *33*, 1141–1152.

Mo, T., M. D. Goldberg, and D. S. Crosby (2001), Recalibration of the NOAA Microwave Sounding Unit, *J. Geophys. Res.*, *106*, 10,145–10,150.

Oke, T. R. (1978), *Boundary Layer Climates*, 2nd ed., pp. 81–84, Methuen, New York.

Rosenkranz, P. W. (1993), Absorption of microwaves by atmospheric gases, in *Atmospheric Remote Sensing by Microwave Radiometry,* edited by M. A. Janssen, John Wiley, Hoboken, N. J.

Schabel, M. C., C. A. Mears, and F. W. Wentz (2003), Stable long-term retrieval of tropospheric temperature time series from the Microwave Sounding Unit, paper presented at International Geoscience and Remote Sensing Symposium, Inst. of Electr. and Electron. Eng., Toulouse, France.

Swanson, R. E. (2003), Evidence of possible sea-ice influence on Microwave Sounding Unit tropospheric temperature trends in polar regions, *Geophys. Res. Lett.*, *30*(20), 2040, doi:10.1029/2003GL017938.

Vinnikov, K. Y., and N. C. Grody (2003), Global warming trend of mean tropospheric temperature observed by satellites, *Science*, *302*, 269–272.

Wald, A. (1940), The fitting of straight lines if both variables are subject to error, *Ann. Math. Stat.*, *11*, 284.

M. D. Goldberg, N. C. Grody, J. T. Sullivan, and J. D. Tarpley, Center for Satellite Applications and Research, NOAA/NESDIS, Camp Springs, MD 20746-4304, USA. (norman.grody@noaa.gov)

K. Y. Vinnikov, Department of Meteorology, University of Maryland, College Park, MD 20742, USA.